Earth Planet. Sci. Lett. 668 (2025) 119549

Contents lists available at ScienceDirect

Earth and Planetary Science Letters

journal homepage: www.elsevier.com/locate/epsl

Ni isotope cycling in sediments of highly productive upwelling systems

Tim Sweere [a,*], Corey Archer [a], Sarah Fleischmann [a], Florian Scholz [c], Peter Kraal [b], Derek Vance [a]

[a] ETH Zürich, Institute of Geochemistry and Petrology, Department of Earth Sciences, Zürich, Switzerland
[b] NIOZ Royal Netherlands Institute for Sea Research, Department of Ocean Systems, and Utrecht University, Den Burg, Texel, the Netherlands
[c] Institute for Geology, Center for Earth System Research and Sustainability, Universität Hamburg, Hamburg, Germany

ARTICLE INFO

Editor name: Dr Tristan Horner

Keywords:
Ni isotopes
Pore waters
Sediment geochemistry
Redox cycling
Benthic flux
Nickel
Upwelling continental margins

ABSTRACT

Nickel is a bio-essential micronutrient in the ocean and the element holds significant potential for the reconstruction of paleoenvironmental conditions. Nickel isotopes provide information on processes controlling internal oceanic cycling and the oceanic mass balance. These insights provide the basis for inferences from the sedimentary record. Recent studies have shown that diagenetic Ni cycling can cause isotope fractionation and may affect the global oceanic dissolved pool, but direct data to constrain such processes in detail remain relatively scarce. Here, we present a large Ni isotope dataset for sediments and pore waters at eight different locations along the Namibian and Peruvian margins, some of the most productive and oxygen-depleted regions in the open ocean. These different stations represent a wide range of depositional redox conditions, allowing evaluation of Ni behaviour in different environments and better constraints on sedimentary Ni cycling and the potential of Ni as a paleo-environmental proxy.

The sedimentary data presented here reinforce findings from previous studies that have suggested that excess Ni burial in organic-rich, strongly reducing sediments underlying highly productive surface waters is unfractionated from the deep ocean isotope composition (1.33 ± 0.07 ‰), with an average $\delta^{60}Ni_{excess}$ of 1.37 ± 0.16 ‰ (1 SD, $n = 74$) for Ni-enriched samples ($f_{excess} > 0.8$). This observation suggests that sedimentary records from organic-rich continental margin upwelling settings can serve as an archive for past deep-ocean $\delta^{60}Ni$ values. The pore water data provide additional constraints on Ni isotope cycling in different redox conditions and show that the preferential precipitation of isotopically light Ni leaves sulphidic pore waters enriched in isotopically heavy Ni, with an average $\delta^{60}Ni$ value of 2.04 ± 0.41. Pore-water Ni concentrations are higher than those in the overlying bottom water, implying a diffusive benthic source in these environments, with an average local flux of -28 μmol m^{-2} yr^{-1}. Where outputs from the oceanic dissolved pool are defined in terms of the characteristics of deeper sediments, this benthic flux should be viewed as recycled, not as a new net input in the oceanic mass balance. With other recent studies, our data highlight benthic Ni fluxes as a feature of highly productive environments despite sulphidic pore waters. However, the observed benthic fluxes in these studies are relatively small compared to sedimentary Ni accumulation rates, suggesting Ni burial is relatively efficient, with 92 ± 7 % (1SD, $n = 11$) of deposited Ni being retained in the sediment.

1. Introduction

Nickel is a bio-essential trace element and exhibits a nutrient-type distribution in the modern ocean (e.g. Bruland, 1980; Middag et al., 2020). These features, as well as variability in the processes that remove Ni from the dissolved pool under different redox conditions, give Ni potential as a tool for palaeoenvironmental reconstruction (e.g. Cameron et al., 2009; Konhauser et al., 2009; Böning et al., 2015; Wang et al., 2019b; Sweere et al., 2023). Ongoing perturbations to the ocean-climate system may affect local or global Ni cycles, for example through ocean deoxygenation, with possible consequences for marine life and ecosystems. Evaluating the effects of such perturbations and the potential of Ni as a reliable palaeoenvironmental tool requires a robust understanding of the global mass balance and relevant processes in the internal Ni cycling in the ocean. We contribute to this understanding by focusing on behaviour of Ni and its isotopes under reducing conditions

* Corresponding author.
E-mail address: tim.sweere@eaps.ethz.ch (T. Sweere).

https://doi.org/10.1016/j.epsl.2025.119549
Received 28 March 2025; Received in revised form 30 June 2025; Accepted 17 July 2025
Available online 31 July 2025

in highly productive upwelling margins.

Nickel plays a crucial role in various enzymes with a large range of functions (Alfano and Cavazza, 2020; Glass and Dupont, 2017; Ragsdale, 2009), perhaps most notably in the nitrogen cycle due to Ni requirement in urease, which catalyses the hydrolysis of urea to ammonia, and indirect involvement in nitrogen fixation. Many strains of cyanobacteria utilise a Ni superoxide enzyme and have a relatively large Ni requirement (C.L. Dupont et al., 2008; C.L. 2010), while the Ni-containing methyl-coenzyme M reductase is key for methanogenesis and the anaerobic oxidation of methane (Scheller et al., 2010).

The behaviour of Ni as a micronutrient is also reflected in its water-column profile, involving low dissolved Ni concentrations near the surface and higher concentrations at depth (e.g. Sclater et al., 1976; Bruland, 1980; Middag, 2020). Unlike most other bio-essential trace elements, however, surface ocean Ni concentrations do not drop much below ~2 nM. It has been proposed that this residual photic zone concentration is due to a biologically unavailable ligand-bound Ni pool (Archer et al., 2020; Dupont et al., 2010; Mackey et al., 2002), or to slow kinetics of uptake (Morel et al., 2006). However, recent culture experiments suggest that the majority of surface ocean Ni, at least 80 %, is labile and available for biological uptake, implying that the residual surface ocean Ni is a result of phytoplankton demand that is lower than for other nutrients (John et al., 2022).

Modern ocean Ni isotope data have revealed a homogenous deep-ocean composition (1.33 ± 0.07 ‰, 1SD, >500 m depth) and significant contrasts between different surface biogeochemical regimes (Archer et al., 2020; Bian et al., 2024a; Cameron and Vance, 2014; 2021; Lemaitre et al., 2022; Takano et al., 2017; Wang et al., 2019a; Yang et al., 2020). Relatively low Ni uptake, and muted surface ocean Ni-isotope fractionation, in the Southern Ocean likely reflects the importance of diatoms in comparison to cyanobacteria, the latter more abundant north of the Polar Front (Archer et al., 2020). Compiled datasets show that surface-ocean Ni isotope fractionation only occurs at low latitudes, leading to δ^{60}Ni values of surface waters up to ~1.7 ‰ (Archer et al., 2020; Yang et al., 2021), and hint at Ni-N co-limitation in the modern ocean (Lemaitre et al., 2022). Nickel has been shown to be bio-limiting in some culture experiments, including for diazotrophic cyanobacteria *Trichodesmium*, which also suggests Ni could possibly be or become (co-)limiting under specific natural conditions (Dupont et al., 2008; Ho, 2013; Price and Morel, 1991).

Rivers (δ^{60}Ni of +0.8 ‰) are considered to be the largest source of Ni to the ocean (Cameron and Vance, 2014; Gueguen and Rouxel, 2021; Little et al., 2020; Revels et al., 2021). Dust and hydrothermal inputs are thought to be small compared to the riverine input. Nickel isotope data from sediments deposited under oxygenated conditions suggest that diagenetic remobilisation of Ni (i.e. reductive dissolution of Mn-oxides) may lead to a recycled benthic flux of isotopically heavy Ni to the ocean in such an environment (Gueguen and Rouxel, 2021; Little et al., 2020). However, in settings with a sufficiently deep oxygen penetration depth and a solid-phase Mn-oxide layer, Ni burial is highly efficient (Bruggmann et al., 2024). Of crucial importance to the oceanic mass balance is the extent to which this benthic flux returns previously dissolved Ni that was temporarily sequestered in the sediment back to the water column (recycled), or whether the flux includes Ni from materials that represent a new source of dissolved Ni to the ocean. Recently, Bian et al. (2024b) argued, on the basis of pore-water data from Mn-reducing sediments on the Pacific margin, that these conditions may mobilise lithogenic Ni, a new source of Ni to the ocean. The evidence for this assertion was a Ni isotope composition in pore water close to that of the upper continental crust, at around δ^{60}Ni = +0.1 ‰. However, Mn-oxides vary in their Ni isotope composition from −1 to over +2 ‰, with sub-oxic sediments such as those in the Bian et al. (2024b) core lying in the range −0.2 to +0.1 (Fleischmann et al., 2023), encompassing the lithogenic value. If the benthic flux only recycles Ni previously removed from the oceanic dissolved pool, then characterisation of the final buried sedimentary pool of Ni, beneath the depth of diagenetic modification and remobilisation, is sufficient to define the net output in the long-term oceanic mass balance (Fleischmann et al., 2023). More studies are required to better understand the role of benthic Ni fluxes in the global Ni mass balance, particularly across diverse environments such as upwelling margins and more oxygenated continental margins.

Today, global outputs of Ni to carbonate and euxinic sediments are thought to be relatively small (Vance et al., 2016; Ciscato et al., 2018; Little et al., 2020; Gueguen and Rouxel, 2021). The Ni output associated with Mn-oxides is the largest sink and can be further divided into sub-sinks with different Ni/Mn ratios and isotope compositions (Gall et al., 2013; Little et al., 2020; Gueguen and Rouxel, 2021; Fleischmann et al., 2023). A recent revision of the Mn-oxide sink recognized the importance of Ni scavenging to Mn-oxides in proximal hydrothermal settings in addition to an abyssal oxic pelagic and a likely small suboxic sink; this allows a balanced global marine Ni isotope budget with a required δ^{60}Ni of the Mn-oxide sink of about +0.45 ‰ (Fleischmann et al., 2023). Organic-rich sediments comprise the second-largest sink for Ni after Mn-oxides. Studies of Peruvian and Namibian Margin sediments suggests that the Ni isotope composition of excess Ni (i.e. non-lithogenic Ni) buried in organic-rich sediments approaches the deep ocean composition (Ciscato et al., 2018; He et al., 2023).

Key aspects of the organic-rich sink are still incompletely understood. Nickel contents in sediments from highly productive continental margin upwelling systems have been shown to strongly correlate with the total organic-carbon content (Böning et al., 2015; Ciscato et al., 2018; Sun et al., 2025). Most of the excess Ni in such sediments can be attributed to phytoplankton uptake and delivery to sediments, with relatively minor contributions from other particulate phases (A. Plass et al., 2021). However, sedimentary Ni:C ratios in these settings are typically much higher than the Ni:C ratio found in phytoplankton, likely due to the preferential retention of Ni as organic carbon is respired and lost back to the water column and sediment (Böning et al., 2015; Ciscato et al., 2018; A. Plass et al., 2021; Bruggmann et al., 2024; Fleischmann et al., 2025).

Fleischmann et al. (2025) used the geochemical and isotope characteristics of anoxic-sulphidic sediments and pore waters from the Kiel Bight in the Baltic Sea, to construct a model whereby Ni retention in such settings occurs through sequestration to a solid sulphide phase. This study, as well as that of Bruggmann et al. (2024), also use pore-water profiles in combination with Ni burial rates to show that a small proportion (10±7 %) of the originally organic-associated Ni is lost back to the water column as a recycled benthic flux. Several recent studies have now highlighted the potential significance of diagenetic cycling of Ni and its isotopes to the marine Ni cycle (Bian et al., 2024b; Bruggmann et al., 2024; Gueguen and Rouxel, 2021; He et al., 2023; Little et al., 2020; Plass et al., 2021; Fleischmann et al., 2025). However, data on the sedimentary redox controls under strongly reducing conditions remain relatively scarce, particularly for two of the major open-ocean upwelling settings where anoxic organic-rich sediments are deposited, Namibia and Peru.

Here, we present Ni isotope data from Namibian and Peruvian Margin sediments and pore waters. These settings feature high organic-carbon burial rates and a large range in depositional redox conditions that allow a detailed assessment of Ni isotope cycling in such environments. In particular, we extend the approach of Fleischmann et al. (2025), so far undertaken only for a small anoxic bay with a limited range of conditions, to these larger-scale open-ocean settings recording substantially greater variability in local redox conditions. Specifically, by comparing Ni isotope data to major nutrient and redox indicators, we evaluate Ni isotope behaviour in the range of redox conditions across these margins, and the relevance of our findings to the global isotopic mass balance of the element.

2. Setting and samples

2.1. Namibian margin

We present data from sediment cores taken from four stations on the Namibian margin, between 23 and 25°S, collected during research cruise 64PE449 with R/V *Pelagia* in February 2019 (see Van Kemenade et al., 2022; Fig. S1 for exact locations and details). The studied stations represent a large range of redox conditions, with a bottom water [O_2] of 179 μmol kg^{-1} for the deepest station to anoxic conditions on the shelf (Table 1). Upwelling of nutrient-rich waters in this area lead to high rates of primary productivity and an extensive OMZ. Hydrogen sulphide (H_2S) release occurs periodically from shelf sediments, particularly during austral spring and summer (Weeks et al., 2004). Shelf sediments consist of diatomaceous and organic carbon-rich muds, with organic carbon contents ranging between 2 and 15 % (Calvert and Price, 1983; Inthorn et al., 2006). For some figures, we include previously published data from the same setting by He et al. (2023), taken from stations further south (~ 26°S).

2.2. Peruvian margin

Sediment cores were collected off the coast of Peru, between April and May 2017 during RV Meteor cruises M136 and M137, at six stations across the Peruvian shelf at a latitude of ~12°S, between 75 m and 250 m water depth (Fig. S2). Further details of the sampling locations are given in A. Plass et al. (2021). On the Peruvian Margin, seasonal upwelling of nutrient-rich water combined with high rates of primary productivity results in an intense OMZ, with essentially anoxic bottom water at water depths between 100 m and 500 m (Thamdrup et al. (2012), and episodic H_2S release from the sediment into the water column (Schunck et. al., 2013). Shelf sediments consist of fine grained diatomaceous and organic carbon-rich hemipelagic muds (e.g. Suess et al., 1987), with organic carbon contents ranging between 3 and 14 % (Plass et al., 2021).

2.3. Sample collection and on-board processing

Namibia: Sediment cores were collected using a multi-corer. The cores were directly capped after collection and transferred to an on-board laboratory container kept at bottom-water temperatures. The cores were processed and sliced anoxically in an N_2-purged glove bag. Pore waters were separated from sediments using centrifugation and subsequently filtered over a 0.45 μm PES filter. Here, data from two cores per station are presented. One core was used solely for all trace-element (isotope) and sedimentary total organic carbon (TOC) analyses, the other for pore-water major nutrient and H_2S analyses. Pore water nutrient concentrations were analysed directly on-board. All other pore-water samples were stored at 4 °C, for later shore-based analyses. The samples taken for trace-element analyses were acidified (to pH ~1) on-board using ultrapure HCl. Sediment samples were stored frozen at −20 °C in aluminium bags flushed with N_2.

Peru: Sediment cores and pore waters were sampled as previously described in Scholz et al. (2011) and Plass et al., 2021. Briefly, short sediment cores were retrieved using a multi-corer and directly processed onboard in cool and anoxic conditions. Pore waters were collected following onboard centrifugation and acidified to pH < 1 with sub-boiled distilled HNO_3. All sediment and pore water samples for onshore analysis were stored at 4 °C.

3. Methods

3.1. Summary of analytical methods

The analytical methods have been described in detail in other recent publications (Archer et al., 2020; Fleischmann et al., 2025; Vance et al., 2016). Here, we provide a short summary of the procedure.

Elemental concentrations were measured using a Thermo Scientific Element XR ICP-MS at ETH Zurich. Pore waters were diluted 20 × with 2 % HNO_3 before analysis. Frozen sediment samples were dried at 60 °C for two days, powdered with an agate pestle and mortar, and ~0.05 g was fully dissolved using a two-step digestion with HNO_3, HF, and HCl. The final solution was diluted 25,000 × with 2 % HNO_3. Accuracy and precision were verified using two secondary multi-element standards (SLRS-6, SGR1), with measured concentrations matching certified values within 5–10 % for most target elements.

Sample aliquots were taken with a total amount of Ni of ~200 ng, where possible, and spiked with a ^{61}Ni–^{62}Ni double spike to achieve a 1:1 spike:sample ratio for later correction of instrumental and procedural mass discrimination (Archer et al., 2020). For Peru margin pore waters, it was necessary to combine samples at the expense of depth resolution, in order to obtain enough Ni for precise isotope analyses. Pore waters were first concentrated using a small version of the Nobias column described in Vance et al. (2016) and Archer et al. (2020). For all samples, Ni was further separated from matrix and interferences using a 3-stage column chromatography procedure (Fleischmann et al., 2025; Sun et al., 2021). Following purification, the samples were oxidised in a H_2O_2–HNO_3 mixture and dissolved in a 2 % (v/v) HNO_3 solution for analysis. The Ni isotope compositions of the purified Ni fractions were analysed using a Thermo Scientific Neptune Plus MC-ICP-MS at ETH Zürich in low-resolution mode following introduction using a Aridus II desolvator. The Ni isotope data are reported in the standard delta notation relative to NIST SRM986.

$$\delta^{60}Ni(\text{‰}) = \left[\frac{\left(\frac{^{60}Ni}{^{58}Ni}\right)_{Sample}}{\left(\frac{^{60}Ni}{^{58}Ni}\right)_{SRM986}} - 1 \right] \times 1000 \quad (1)$$

Reproducibility was assessed via repeated analyses of secondary standards USGS NodA1 and NodP1. Over the past 10 years, these standards have yielded $\delta^{60}Ni$ values of 1.04 ± 0.07 ‰, (2 SD, n = 489) and 0.35 ± 0.08 ‰, (2 SD, n = 664), respectively. The uncertainties shown on all figures are the long-term reproducibility (±0.08), unless the internal uncertainty is larger, in which case the latter is shown.

The Namibian Margin NH_4^+ samples were kept under N_2 at 4 °C and analysed on board within 6–12 h using a QuAAtro39 gas segmented

Table 1
Basic characteristics of the studied stations. The oxygen concentrations represent data for the deepest CTD sample, ~5–10 m above the seafloor.

Margin	Cruise	Station	Date	Latitude	Longitude	Depth	[O_2]
			[dd-mm-yyyy]	[°S]	[°E]	[mbss]	[μmol kg^{-1}]
Namibia	64PE449	1	03–02–2019	24.056	12.843	1517	179
Namibia	64PE449	2	04–02–2019	24.033	13.132	750	105
Namibia	64PE449	3	01–02–2019	23.096	14.129	136	20
Namibia	64PE449	6	08–02–2019	25.072	14.596	100	<5
Peru	M136/M137	1	Apr/May 2017	12.225	77.180	75	<5
Peru	M136/M137	3	Apr/May 2017	12.278	77.249	130	<5
Peru	M136/M137	5	Apr/May 2017	12.358	77.362	195	<5
Peru	M136/M137	6	Apr/May 2017	12.388	77.703	245	<5

continuous-flow analyzer by Seal Instruments, with a detection limit of 0.019 µmol L^{-1} (Kraal et al., 2025). Pore-water samples for H_2S were kept in glass vials with gas-tight lids, preserved in 1 % zinc acetate/10 mM NaOH and stored at 4 °C until on-shore analysis using the spectrophotometric method of Cline (1969).

3.2. Lithogenic corrections

To evaluate Ni burial in excess of lithogenic Ni in these settings, we calculate the excess Ni fraction (f_{excess}), contents (Ni_{excess}), and isotope composition $\delta^{60}Ni_{excess}$ as follows:

$$f_{excess} = 1 - \left([Ni/Al]_{lith} \times Al_{bulk}\right)/Ni_{bulk} \quad (2)$$

$$Ni_{excess} = Ni_{bulk} - \left([Ni/Al]_{lith} \times Al_{bulk}\right) \quad (3)$$

$$\delta^{60}Ni_{excess} = \frac{\delta^{60}Ni_{bulk} - (1 - f_{excess}) \times \delta^{60}Ni_{lith}}{f_{excess}} \quad (4)$$

where $[Ni/Al]_{lith}$ reflects the Ni/Al ratio of lithogenic material. The average upper continental crust composition, typically taken as an estimate to constrain the lithogenic background, has a Ni/Al ratio of 5.8×10^{-4} (Rudnick and Gao, 2003), but local lithogenic background values may vary considerably. Correlations of Ni/Al with TOC can be used to constrain apparent local lithogenic background Ni/Al values and lead to estimates between 0 and 3.3×10^{-4} for the Peru Margin (Böning et al., 2012). A previous study on the Ni-isotope composition of Namibian margin sediments has therefore used a Ni/Al_{lith} value of 3.3×10^{-4}, as a maximum estimate of lithogenic contributions to this area (He et al., 2023). However, a later study that sought to constrain the local lithogenic background of Namibian Margin sediments directly, highlights the large regional variability and suggests a Ni/Al_{lith} of 5.2×10^{-4} for 25°S, based on Sossuvlei particles (Gäng et al., 2023), a value closer to that of the average upper continental crust composition. To evaluate the uncertainty associated with estimates of Ni_{excess} and $\delta^{60}Ni_{excess}$ that come with heterogenous lithogenic compositions and sometimes unknown local lithogenic background values, we therefore use two different $[Ni/Al]_{lith}$ values for the lithogenic corrections in the presentation of our data in Figs. 1 and 2 (Böning et al., 2012). $\delta^{60}Ni_{lith}$ reflects the Ni-isotope composition of the lithogenic background, for which we use a value of 0.12 ± 0.11 ‰ (1 SD, Cameron et al., 2009; Revels et al., 2021).

3.3. Flux calculations

Diffusive fluxes of Ni across the sediment-water interface are calculated using Fick's first law:

$$Flux = -\phi D_{sed} \frac{dC}{dz}$$

where ϕ is porosity, D_{sed} the effective sedimentary diffusion coefficient (D_{sed}), and $\frac{dC}{dz}$ the concentration gradient for Ni in pore waters. Here, $\frac{dC}{dz}$ reflects the concentration difference between the bottom water and top pore water sample divided by the depth of that pore water sample. D_{sed} denotes the effective molecular diffusion coefficient of Ni in the sediment, and is determined using the seawater diffusion coefficient (D_{sw}) as follows:

$$D_{sed} = \frac{D_{sw}}{\theta^2}$$

where the tortuosity (θ^2) was calculated after Boudreau (1996):

$$\theta^2 = 1 - \ln\left(\phi^2\right)$$

The seawater diffusion coefficient was taken from Yuan-Hui and Gregory, 1974, and adjusted to local temperature, pressure, and salinity using the Stokes-Einstein equation (Boudreau, 1997). Fluxes for the Peru margin stations were previously determined by A. Plass et al. (2021).

4. Results

4.1. Bulk sediment chemistry

Sedimentary total organic carbon (TOC) contents are generally high,

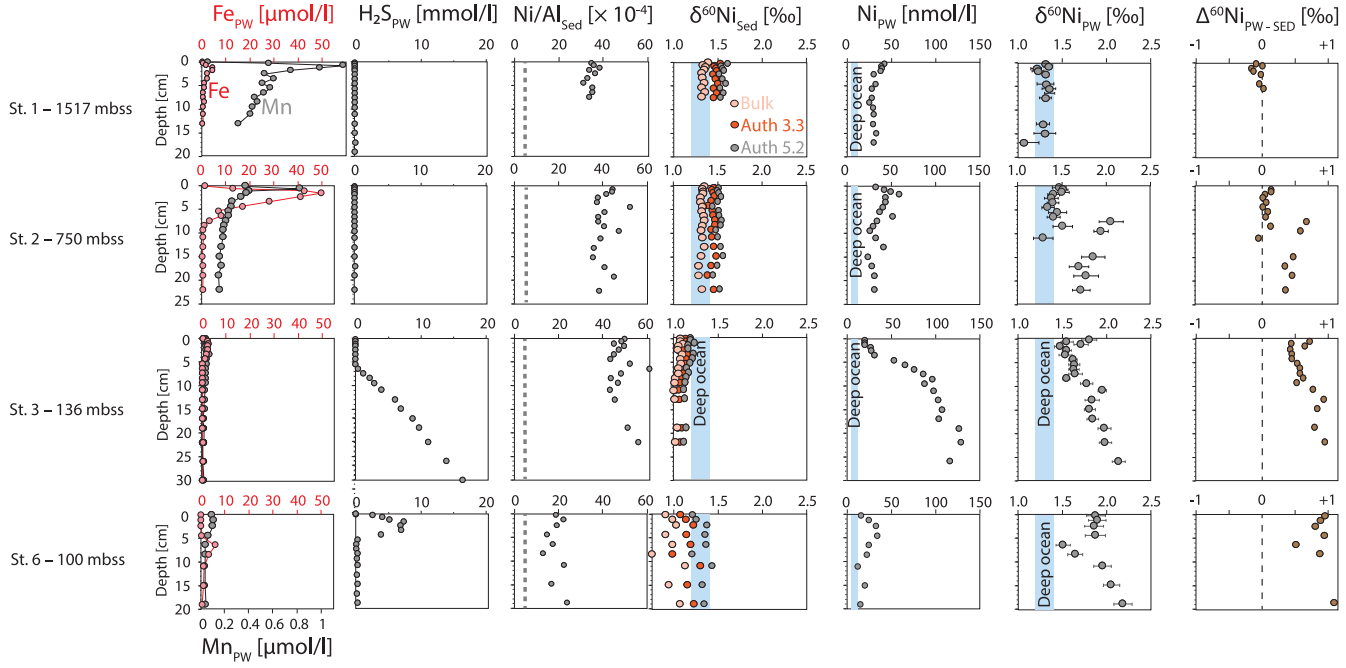

Fig. 1. Depth profiles of Namibian margin sediment and pore water data. The dashed line in the Ni/Al plots shows the likely lithogenic background value of 5.2×10^{-4} g/g (Gäng et al., 2023). In the $\delta^{60}Ni_{sed}$ plot, two values of the Ni/Al lithogenic ratio (3.3 and 5.2×10^{-4}) are used to calculate sedimentary excess Ni isotope compositions. The blue bar represents the average Ni concentration or isotope value of the deep ocean. $\Delta^{60}Ni_{PW\text{-}SED}$ reflects the difference in $\delta^{60}Ni$ values between pore waters and sediments of the same depth ($\Delta^{60}Ni_{PW\text{-}SED} = \delta^{60}Ni_{pore\ water} - \delta^{60}Ni_{sediment}$).

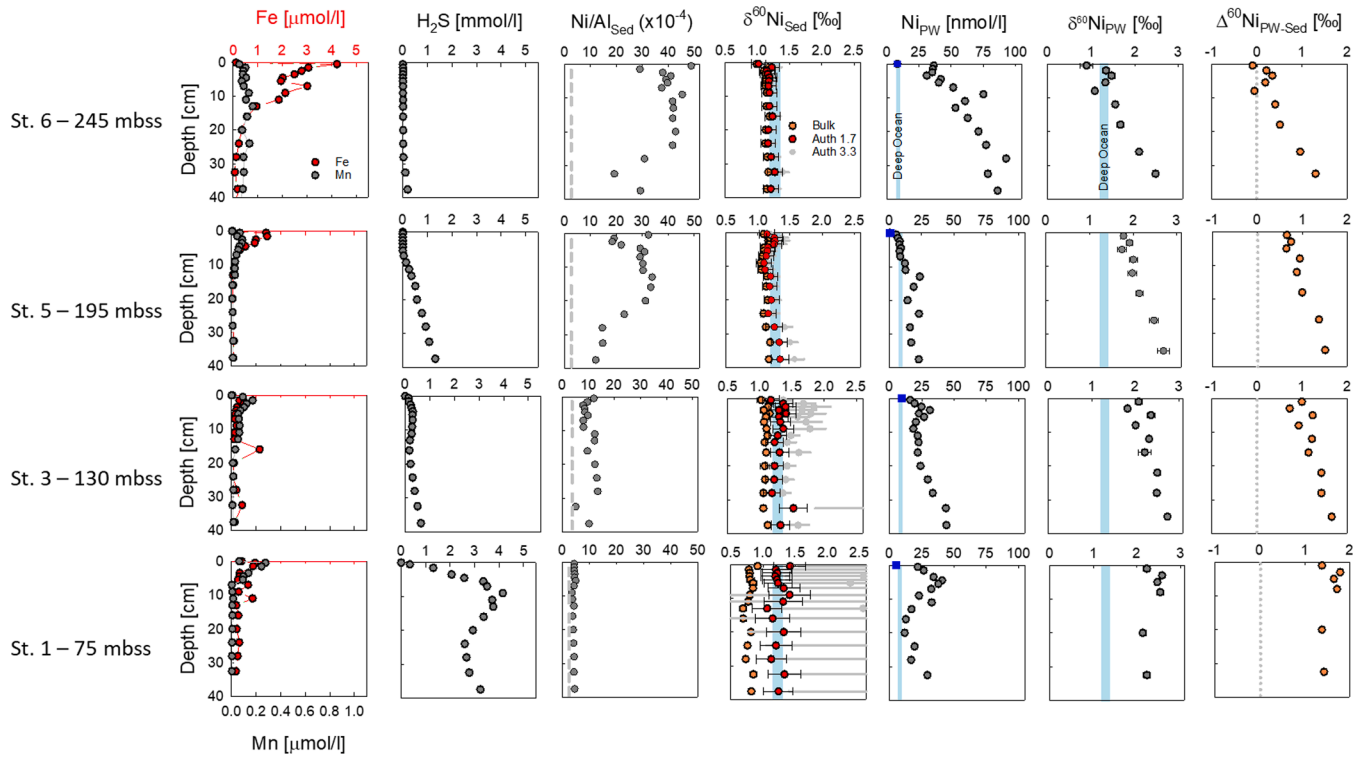

Fig. 2. Depth profiles of Peruvian margin sediment and pore water data. The dashed line in the Ni/Al plots shows the likely maximum lithogenic background value of 3.3 × 10^{-4} g/g. In the $\delta^{60}Ni_{sed}$ plot, two values of the Ni/Al lithogenic ratio (1.7 and 3.3 × 10^{-4}) are used to calculate sedimentary excess Ni isotope compositions. The value chosen to correct bulk Ni isotope compositions for the detrital contribution has a significant impact for samples with lower excess Ni contents, and indeed is likely station specific (see text for details). The blue bar represents the average Ni concentration or isotope value of the deep ocean. $\Delta^{60}Ni_{PW\text{-}SED}$ reflects the difference in δ^{60}Ni values between pore waters and sediments of the same depth ($\Delta^{60}Ni_{PW\text{-}SED} = \delta^{60}Ni_{pore\ water} - \delta^{60}Ni_{sediment}$). The [$H_2S$] data are from Plass et al. (2020). Pore-water Ni concentration data have also previously been published by A. Plass et al. (2021) but the data presented here reflect newly generated data in this study to allow direct comparison with the Ni-isotope data on the same sample aliquots.

with an average of 7.6 ± 3.8 % (1 SD, n = 130). The highest TOC contents are found for the mid-depth stations on the Peruvian margin (195 and 240 m water depth), whereas the lowest values are generally found at the deeper slope stations on the Namibian Margin (stations 1 and 2, at 1517 and 750 m water depth) and the shallowest Peru Margin station (75 m depth). The large range in observed pore water Mn (15 to 1176 nM), Fe (0.05 to 43 µM), and H_2S (0 to 17 mM) concentrations illustrate the range in studied sediment redox conditions. The most strongly reducing conditions generally occur on the shelves, where pore waters become strongly sulphidic at shallow sediment depths. Pore waters from stations 1 and 2 on the Namibian margin show the least reducing conditions, with high NO_3^- concentrations (> 20 µM) just below the sediment-water interface and no (St. 1) or very little (St. 2) detectible accumulation of H_2S at depth.

4.2. Solid-phase nickel contents and isotope composition

Sedimentary Ni contents show an average of 55 ± 28 ppm (1 SD, n = 133); bulk sediment Ni-isotope compositions show a relatively small range, with an average of 1.10 ± 0.17 ‰ (1 SD, n = 116). These values are similar to results from previous studies of these settings, which reported averages of 0.88 ± 0.24 ‰ (1 SD, n = 42) and 1.12 ± 0.08 ‰ (1 SD, n = 25) for Namibian and Peruvian Margin sediments, respectively (Ciscato et al., 2018; He et al., 2023). The observed variability in δ^{60}Ni largely reflects differences between stations, as down-core δ^{60}Ni values are relatively constant (Fig. 1, 2). Low δ^{60}Ni values are predominantly found in sediments from shallower stations.

4.3. Pore-water nickel concentrations and isotope composition

Ni concentrations in pore waters are typically higher than in seawater with an average of 46 ± 28 nM (1 SD, n = 90). Compared to the solid phase, pore waters show a larger range in Ni isotope compositions, with an average δ^{60}Ni value of 1.77 ± 0.41 ‰ (1 SD, n = 90), higher than the modern deep ocean composition (1.33 ± 0.07 ‰) and also higher than recently reported pore-water values of 0.87 ± 0.41 ‰ for Namibian margin pore waters (1 SD, n = 36) (He et al., 2023). Observed δ^{60}Ni values reach a maximum of 2.75 ‰, which is amongst the highest ever observed in natural samples and similar to recently published pore-water data from the southern Californian margin (Bian et al., 2024b). In contrast to the sediments, pore waters show significant and consistent down-core changes, with higher Ni concentrations and δ^{60}Ni values generally observed at greater sediment depths.

Generally positive correlations are observed between $[Ni]_{PW}$ and $[Ni]_{sed}$ and between $\delta^{60}Ni_{PW}$ and $\delta^{60}Ni_{sed}$ (Fig. 3). This comparison also highlights the high Ni concentrations and δ^{60}Ni values of both the studied sediment and pore-water samples in comparison to previously published data (He et al., 2023). The difference in δ^{60}Ni values between pore waters and sediments of the same depth ($\Delta^{60}Ni_{PW\text{-}SED} = \delta^{60}Ni_{pore\ water} - \delta^{60}Ni_{sediment}$) typically increases with increasingly reducing conditions (Fig. 1, 2): low $\Delta^{60}Ni_{PW\text{-}SED}$ values of around 0 ‰ are found in the most oxygenated depositional conditions of station 1 in Namibia and for mildly reducing stations at shallow depths, whereas higher $\Delta^{60}Ni_{PW\text{-}SED}$ values of around 1 ‰ or more are found for samples from strongly sulphidic conditions.

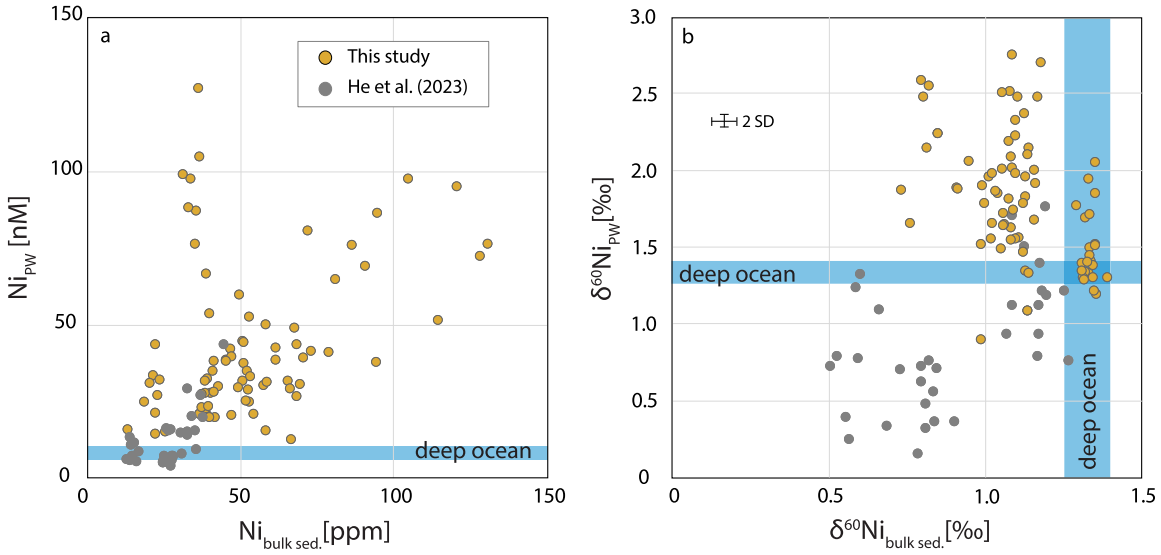

Fig. 3. Comparison of [Ni] and δ^{60}Ni sediment and pore water data. The data presented here show typically high [Ni] and δ^{60}Ni values in both sediments and pore waters compared to previously published data from the Namibian margin.

5. Discussion

5.1. The Ni-isotope composition of margin sediments

The observed variability in $\delta^{60}Ni_{bulk}$ values of upwelling margin sediments can largely be explained by two-component mixing between lithogenic (δ^{60}Ni ~ 0.12 ‰) and authigenic or biogenic end-member with a δ^{60}Ni value close to the seawater composition (Fig. 4), as previously suggested by Ciscato et al. (2018) and He et al. (2023). Calculated $\delta^{60}Ni_{excess}$ values converge to the $\delta^{60}Ni_{seawater}$ value with increasing fraction of excess Ni (f_{excess}) (Fig. S3). The accuracy of the calculated excess Ni estimates depends on the choice of Ni/Al_{lith} ratio, which is known to vary regionally in the modern ocean, and locally at the spatial scale of the Peruvian and Namibian margins (Böning et al., 2012; Gäng et al., 2023). High $\delta^{60}Ni_{excess}$ values for some of the Peruvian margin samples with low f_{excess}, for the maximum value for Ni/Al_{lith} found in the Peru Margin ($= 3.3 \times 10^{-4}$), suggest that these calculations overestimate the contribution of lithogenic Ni to these samples (Fig. 2). A Ni/Al_{lith} value of 1.7×10^{-4} seems to more accurately reflect the local lithogenic background Ni/Al_{lith} for these samples (Böning et al., 2012; Fig. S3). Using best available estimates of regional Ni/Al values of the lithogenic background, 5.2 and 1.7×10^{-4} for the Namibian and Peruvian margins (Böning et al., 2012; Gäng et al., 2023), respectively, the average $\delta^{60}Ni_{excess}$ of the studied samples is 1.30 ± 0.15 (1 S.D., n = 116). However, considering the variable lithogenic composition, $\delta^{60}Ni_{excess}$ values for sediments with low excess Ni cannot be accurately

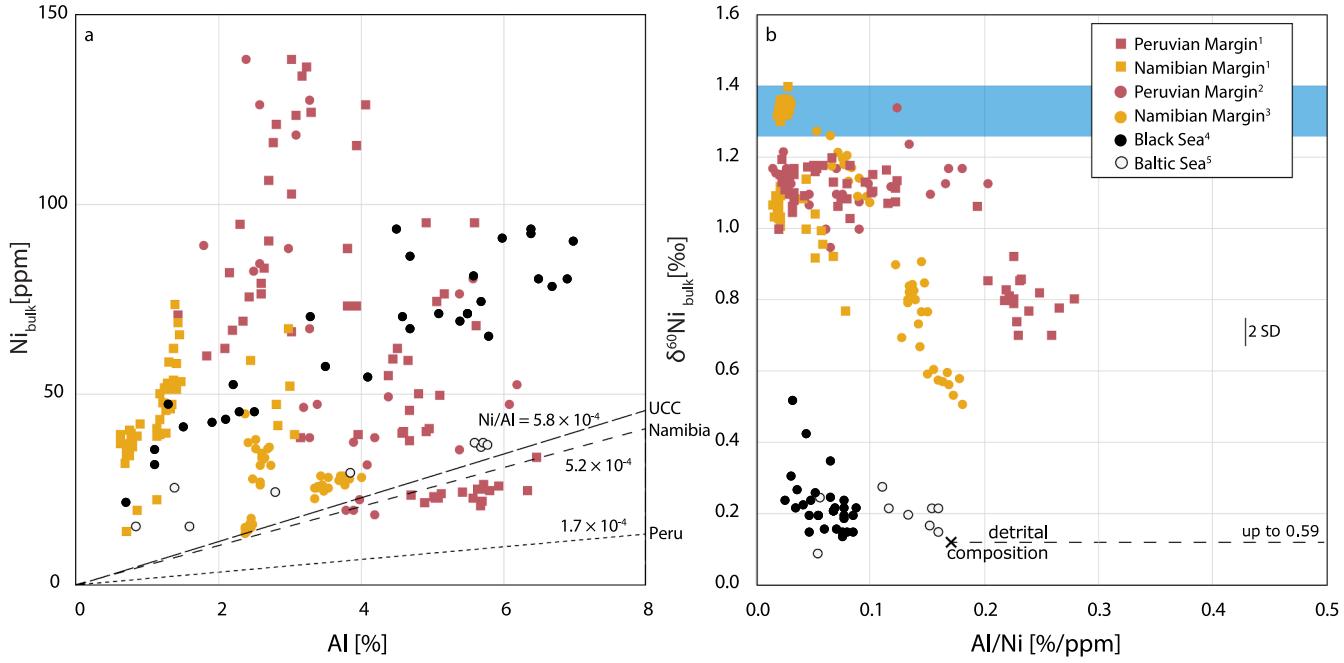

Fig. 4. Lithogenic contributions to sedimentary [Ni] and δ^{60}Ni. (a) All studied samples are enriched relative to estimates of regional lithogenic backgrounds (Böning et al., 2012; Gäng et al., 2023); UCC denotes the upper continental crust composition (Rudnick and Gao, 2003). (b) Most of the variability in sedimentary δ^{60}Ni of margin sediments can be explained by mixing between lithogenic Ni (δ^{60}Ni = 0.12 ‰) and a sedimentary phase with a δ^{60}Ni value that captures the deep ocean composition. [1]This study; [2]Ciscato et al. (2018); [3]He et al. (2023); [4]Vance et al. (2016); [5]Fleischmann et al. (2025).

determined unless local lithogenic background Ni/Al values can be better constrained (Fig. S3; Gäng et al., 2023). In order to better constrain the Ni-isotope composition of the excess Ni end-member, we therefore focus on samples with high (>80 %) excess Ni only. Assuming a relatively high lithogenic Ni/Al for all samples (5.8×10^{-4}, average upper continental crust, Rudnick and Gao, 2003), $\delta^{60}Ni_{excess}$ values for all available Peru and Namibian margin data show an average of 1.37 ± 0.16 ‰ (1 SD, $n = 74$), indistinguishable from the modern deep ocean composition at $\delta^{60}Ni = 1.33 \pm 0.13$ ‰ (Lemaitre et al., 2022).

The uncertainties discussed above do not allow meaningful interpretation of small deviations from the deep-ocean value $\delta^{60}Ni_{excess}$ values. Overall, the strong Ni-TOC correlation in these settings suggests that most excess Ni is delivered to the seafloor in association with organic matter (Böning et al., 2015; Ciscato et al., 2018; Fig S4). With $\delta^{60}Ni_{excess}$ values being close to the deep-ocean composition, this observation implies that little to no isotope fractionation is expressed during surface ocean Ni uptake or other associations with the organic-carbon fraction, either due to removal of a large proportion of bio-available Ni from the surface ocean and/or small fractionation factors associated with these processes (Ciscato et al., 2018; He et al., 2023). Notably, in contrast to all samples from open-ocean upwelling margins, organic-rich sediments from the Black Sea *do* show significant isotope fractionation from the seawater composition. This contrast suggests a fundamental difference in Ni isotope cycling in these two different environments, likely associated with delivery of light Ni to the deep Black Sea by a Mn-particulate shuttle, and/or the subsequent precipitation of Ni-S complexes in deep sulphidic waters (Vance et al., 2016).

In summary, our extensive dataset from the two major modern upwelling systems reinforces suggestions from previous studies (Ciscato et al., 2018; He et al., 2023) that the $\delta^{60}Ni$ of excess Ni buried in highly productive continental margins is the same as the deep-ocean isotope composition, for a large range of local depositional redox conditions.

5.2. Controls on pore water [Ni] and $\delta^{60}Ni$

The pore water Ni concentrations and $\delta^{60}Ni$ data are more difficult to understand as there are different potential diagenetic sources and sinks of Ni that can contribute to the pore water isotope mass balance, not all of them well constrained (see He et al., 2023). However, the reasonably large dataset presented here allows us to interrogate some of these controls through: 1) assessment of different potential sources of Ni to pore waters by comparison to other elemental concentrations and ratios and; 2) evaluation of redox controls on pore water $\delta^{60}Ni$ by comparison of data from different redox zones.

5.2.1. Sources of Ni to pore waters

Data for pore water Ni concentrations are plotted versus NH_4^+ in Fig. 5, to assess the extent to which pore water Ni concentrations can be attributed to organic matter remineralization. The more reducing stations (neither nitrogenous nor Mn-rich) at both Peru and Namibia show positive correlations between pore water [Ni] and [NH_4^+], similar to recent observations from Baltic Sea sediments (Fleischmann et al., 2025). Moreover, there is a correspondence between the Ni/NH_4^+ ratio and the redox state of the pore water. In sediments off Peru, the highest ratio is seen at station 6 (least reducing) for which the Ni/NH_4^+ is similar to estimates for the stoichiometric ratio in phytoplankton, as derived from dissolved surface ocean concentrations (Ni/N of 0.06–0.11 mmol/mol; Fig. 5; Twining and Baines, 2013). This likely reflects the dominance of organic matter deposition and subsequent degradation in surface sediment as a source of both Ni and NH_4^+ to pore water. At the stations off Peru with more sulphidic chemistry, the arrays of data on Fig. 5 fall progressively further below this stoichiometric ratio. The two stations off Namibia with sulphidic sediment conditions (stations 3 and 6) also plot below the phytoplankton ratios, albeit to a lesser extent than the sediments from stations off Peru. For Namibia, two of the stations are significantly less reducing than at Peru (nitrogenous station 1 and high dissolved Mn in station 2 on Fig. 5) and are discussed separately below.

Pore water $\delta^{60}Ni$ values for samples with relatively high Ni concentrations (i.e. high Ni/NH_4^+) cluster closely around the seawater value (Fig. 6a). This observation suggests that most Ni released to pore waters by the oxidation of organic matter is unfractionated from the seawater composition, consistent with the observation that excess sedimentary Ni captures the seawater isotope composition in these settings. The samples that feature Ni/NH_4^+ ratios considerably below estimates of the stoichiometric ratios (Fig. 5, 6a), suggesting the removal of Ni from solution, have heavier isotope compositions. These samples are largely from sulphidic pore waters (Fig. 5) and have $\delta^{60}Ni$ values of 1.85 ± 0.39 (1 SD, $n = 77$), highlighting the control of sulphide formation on pore water $\delta^{60}Ni$ by preferential removal of isotopically light Ni with

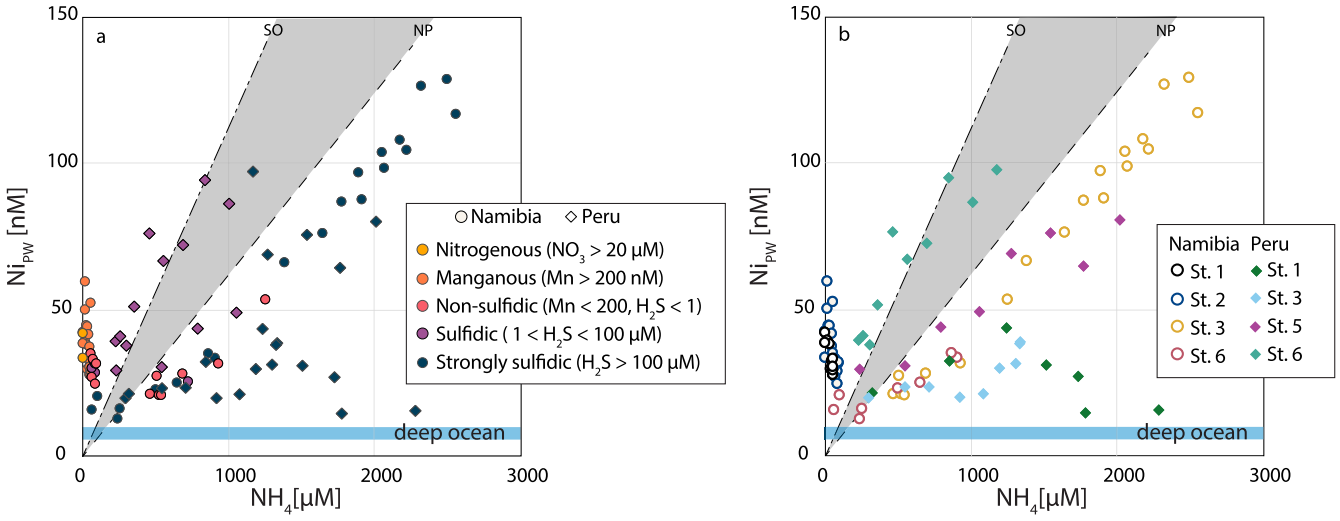

Fig. 5. Controls on pore water [Ni]. For several of the studied stations, pore water [Ni] is positively correlated with NH_4^+, though with different gradients for different stations. The dashed lines reflect the Ni/N stoichiometries of surface ocean uptake in the North Pacific (NP) and Southern Ocean (SO), as calculated from dissolved upper ocean Ni and P concentrations (Twining and Baines, 2013), assuming a P:N ratio of 1:16. Estimates of Ni/N stoichiometries from the North Atlantic fall within this range. Ni/NH_4^+ ratios of samples from mildly reducing stations typically show values close to their stoichiometric ratios, whereas ratios for samples from the most reducing conditions are generally lower. Data for nitrogenous and Mn-rich stations plot at higher Ni concentrations than Ni-NH_4 stoichiometry would suggest. The Peru Margin NH_4^+ data are from Dengler and Sommer (2017) and Sommer and Dengler (2019).

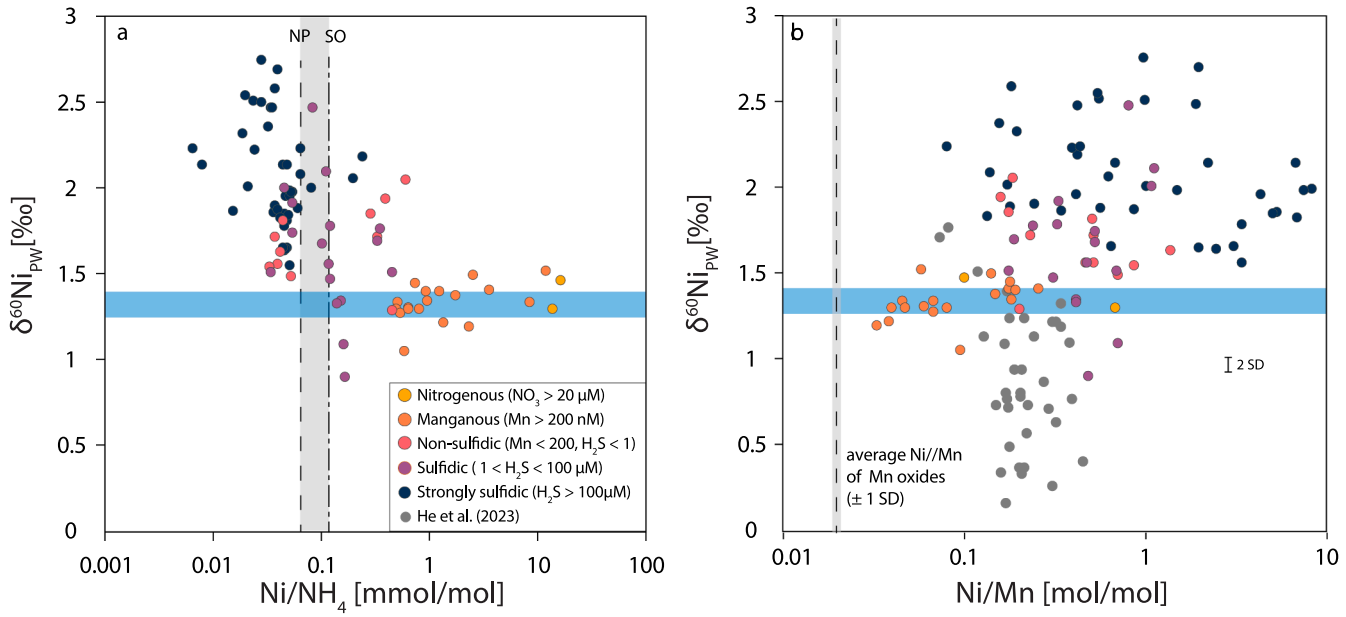

Fig. 6. Evaluation of pore water Ni sources and sinks and their impact on δ^{60}Ni. Ni/NH_4 (a) ratios provide constraints on the amount and isotope composition of Ni contributions to pore waters from the remineralisation of organic matter. The dashed lines reflect the Ni/N stoichiometries of surface ocean uptake in the North Pacific (NP) and Southern Ocean (SO), as calculated from dissolved upper ocean Ni and P concentrations (Twining and Baines, 2013), assuming a P:N ratio of 1:16. Estimates of Ni/N stoichiometries from the North Atlantic fall within this range. Ni/Mn (b) ratios provide some additional information on the contribution of Ni to pore waters from the reductive dissolution of Mn-oxides. The Ni/Mn ratio of Mn-oxide rich abyssal sediments is indicated for comparison (Fleischmann et al., 2023). Combined, these figures suggest that, in the studied settings, both Mn-oxides and organic-matter release Ni to pore waters with an isotopic composition close to the seawater composition. The observed trends to higher δ^{60}Ni with lower Ni/NH_4 can be explained by precipitation as or with sulphides.

sulphides (Fleischmann et al., 2025, discussed further in Section 5.2.2). Combined, these observations suggest that most observed variation in [Ni] and $\delta^{60}Ni_{PW}$ can be explained by 1) Ni release from organic matter oxidation, with an isotope composition equal to the seawater composition, and 2) preferential removal of isotopically light Ni during sulphide precipitation.

Pore-water samples from nitrogenous and Mn-rich cores (stations 1 and 2 on the Namibia margin), on the other hand, show $Ni:NH_4^+$ ratios that lie to the left of the stoichiometric ratio (Fig. 5) and large variability in Ni_{PW} concentrations that correlates poorly with $[NH_4^+]$. This observation suggests a significant contribution of Ni from other sedimentary phases, e.g. reductive Mn-oxide dissolution, or the preferential removal of NH_4^+, e.g. by oxidation. Pore-water Ni/Mn ratios extend towards those for Mn-oxide rich abyssal sediments (Fig. 6b), suggesting that Ni delivery to the pore waters by reductive Mn-oxide dissolution is substantial for those samples (Fig. 7). δ^{60}Ni values of pore waters with Ni/Mn ratios close to dispersed Mn-oxides are comparable to those of the deep ocean.

5.2.2. *Sinks of Ni from pore waters*

With the two main sources of Ni to the studied pore waters apparently having an isotope composition close to the deep ocean, the main cause for variation in $\delta^{60}Ni_{PW}$ must arise from fractionation associated with removal of Ni. The Ni isotope compositions of pore waters with relatively high Mn concentrations (for our purpose defined as [Mn] > 200 nM) vary around the seawater composition with an average of 1.38 ± 0.23 ‰ (1 SD, $n = 20$). These mildly reducing conditions therefore do not appear to lead to the preferential removal of isotopically light or heavy Ni. By contrast, samples from strongly sulphidic conditions (here as $[H_2S] > 100$ µM) are almost exclusively isotopically heavier than the seawater composition, and show an average δ^{60}Ni of 2.04 ± 0.41 ‰ (1 SD, $n = 43$), similar to deep Black Sea dissolved δ^{60}Ni values (1.89 ± 0.15 ‰, Vance et al., 2016) and recently reported values from other sulphidic pore waters (up to 2.3–2.4 ‰, Bruggmann et al., 2024; Fleischmann et al. 2025). In addition to these previous observations, our new data therefore suggest that the preferential removal of isotopically light Ni associated with sulphide precipitation is a key control on pore-water δ^{60}Ni in these settings. The fractionation factor for this process cannot be precisely constrained with the presented data due to the variable release of Ni to pore waters from sedimentary sources, leading to a lot of scatter in the [Ni] data (Fig. 8a). Recognizing that there are variable sources of Ni to pore waters in addition to removal and loss through a benthic efflux, and that the coupled supply of Ni and NH_4^+ from organic matter respiration is the most important, normalisation to NH_4^+ removes some but not all of the scatter (Fig. 8b; Fleischmann et al. 2025).

With sulphide precipitation as a key removal mechanism of Ni from pore waters, it is initially somewhat surprising that the strongly sulphidic conditions observed here do not lead to very significant drawdown of the dissolved Ni pool. We note that in this particular case, there are both sources sinks of Ni to pore waters, as discussed above, so that aqueous concentrations will depend on the relative rates of the two processes. The suggestion that rates of removal to sulphide are slow is supported by the fact that incomplete Ni drawdown is a common feature of sulphidic waters. This feature has been observed previously for sulphidic pore waters from the Baltic Sea (Fleischmann et al., 2025), as well as deep waters in sulphidic basins like the Black Sea (e.g. Landing and Lewis, 1991; Vance et al., 2016) and anoxic fjords (e.g. Jacobs et al., 1985). The lack of major drawdown of the Ni dissolved pool likely reflects slow removal versus rapid supply, the former perhaps due to the specific ligand exchange reaction kinetics and redox reaction pathways (Morse and Luther, 1999). Thus, while the details of Ni removal in sulphidic conditions require further investigation, most of the variation in the δ^{60}Ni and [Ni] of pore waters presented here can be ascribed to 1) variable release of dissolved Ni from the sediment, unfractionated from seawater, and 2) preferential removal of isotopically light Ni associated with sulphide precipitation. Such a framework, however, does not provide an explanation for the comparatively low [Ni] and $\delta^{60}Ni_{PW}$ found previously for Namibian Margin sediments from 26°S (Fig. 8a; He et al., 2023), discussed in the next section.

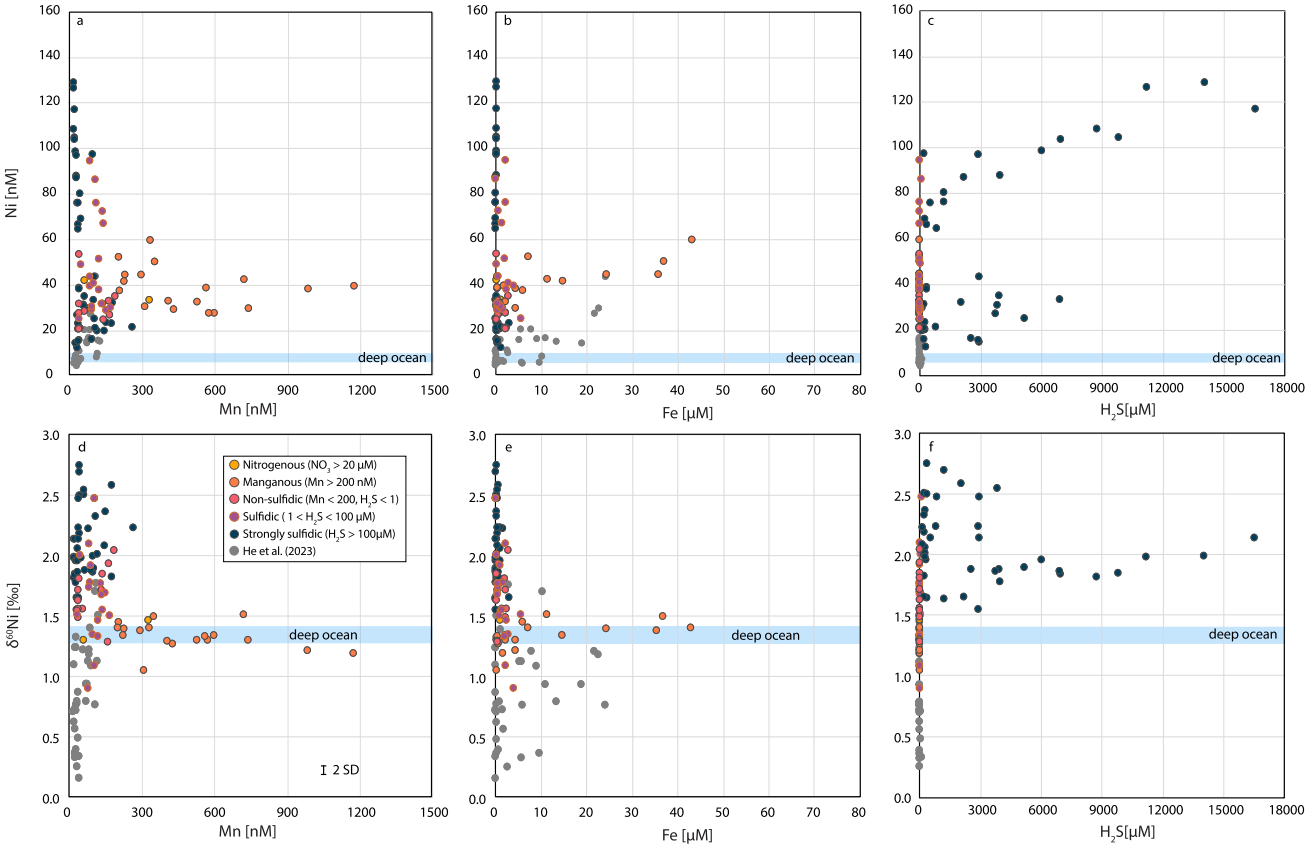

Fig. 7. Pore water [Ni] and δ^{60}Ni in different redox zones. Pore water [Ni] and δ^{60}Ni values plotted against reaction products of sedimentary redox reactions, with the aim of assessing redox controls on [Ni] and δ^{60}Ni. There is no clear or consistent correlation between [Ni] and these reaction products, apart from high [Ni] occurring in strongly sulphidic conditions, suggesting that redox conditions are not the dominant control on pore water [Ni]. Samples with high Mn concentrations generally show δ^{60}Ni values close to the deep ocean composition whereas high δ^{60}Ni values are observed for samples with high H_2S concentrations (sulphidic conditions). Ferruginous conditions (high [Fe]) show δ^{60}Ni values similar to the deep ocean composition or lower.

5.2.3. *Controls on low pore water δ^{60}Ni values*

The previously published Namibian margin pore-water data from ~26°S (He et al., 2023) exhibit notably lower δ^{60}Ni values compared to the other pore water data, even for those from similar redox conditions (Fig. 6–8). One explanation for this lies in the small dissolved Ni pool for these samples, which can be more easily shifted to lower δ^{60}Ni values by small additions of isotopically light Ni or removal of isotopically heavy Ni from solution. Positive relationships of $\delta^{60}Ni_{PW}$ and $[Ni]_{PW}$ with $\delta^{60}Ni_{sed}$ and $[Ni]_{sed}$ suggest that these low pore water δ^{60}Ni values can at least partly be attributed to the composition of the sediment (Fig. 3). In these samples, both the bulk and excess sedimentary Ni contents are relatively low compared to the other data, likely due to low TOC contents (Fig. S4), resulting in lower concentrations of Ni in the pore water. Additions of isotopically light Ni from the dissolution of Mn-oxide or detrital minerals to a small dissolved Ni pool may shift $\delta^{60}Ni_{PW}$ values from the seawater composition towards lower values (Fig. 8a). The source of the isotopically light Ni to these pore waters is relevant because if it is derived from the dissolution of lithogenic material, a benthic flux to the seawater would provide a net input to the global mass balance (Bian et al., 2024b). Alternatively, preferential removal of an isotopically heavy Ni phase from a seawater composition can, in principle, also explain the low $\delta^{60}Ni_{PW}$ values for this group of samples, though this seems unlikely since there is no direct mechanistic explanation for such a change.

Overall, pore water [Ni] and δ^{60}Ni data remain difficult to interpret as it is likely a dynamic and transient pool with different sources and sinks. However, the large dataset presented here highlights some key controls: 1) sediment composition is important for pore water Ni, where low excess Ni contents lead to lower dissolved [Ni] and δ^{60}Ni; 2) excess Ni, largely associated with organic matter in these settings, is unfractionated from seawater; 3) no observable fractionation occurs upon release to pore waters; 4) sulphide precipitation is clearly a key control on pore water δ^{60}Ni for the reducing stations, removing isotopically light Ni from solution, and 5) removal of Ni with sulphides does not draw down the dissolved pore water pool completely, leaving pore waters enriched in Ni and thereby resulting in a diffusive benthic flux of Ni out of the sediment.

5.3. *Burial fluxes, benthic effluxes and mass balance*

High pore-water concentrations imply significant diffusive benthic fluxes from sediment to bottom waters for all but one of the studied stations (Table S1, Fig 9a). Following the procedure described in the methods section, the Ni fluxes obtained vary from −71 to +2.6 μmol m^{-2} yr^{-1} (negative values denote a flux out of sediment), with an average of −28 and median of −18 μmol m^{-2} yr^{-1}. These values are comparable to recently published data from the Soledad station on the Mexican continental margin (−28 μmol m^{-2} yr^{-1}, Bruggmann et al., 2024), and for the southwestern Baltic Sea (average of −10.8 μmol m^{-2} yr^{-1}, Fleischmann et al. 2025). The highest benthic fluxes are found from pore waters that remain nearly completely non-sulphidic for the studied depths (stations 1 and 2 from the Namibian margin, and station 6 from the Peruvian Margin). For these stations, there is no specific evidence for a significant contribution from the dissolution of terrigenous material to the dissolved pore water Ni pool. This finding is in contrast to the suggestion made by Bian et al. (2024b) for stations where Mn reduction occurs in

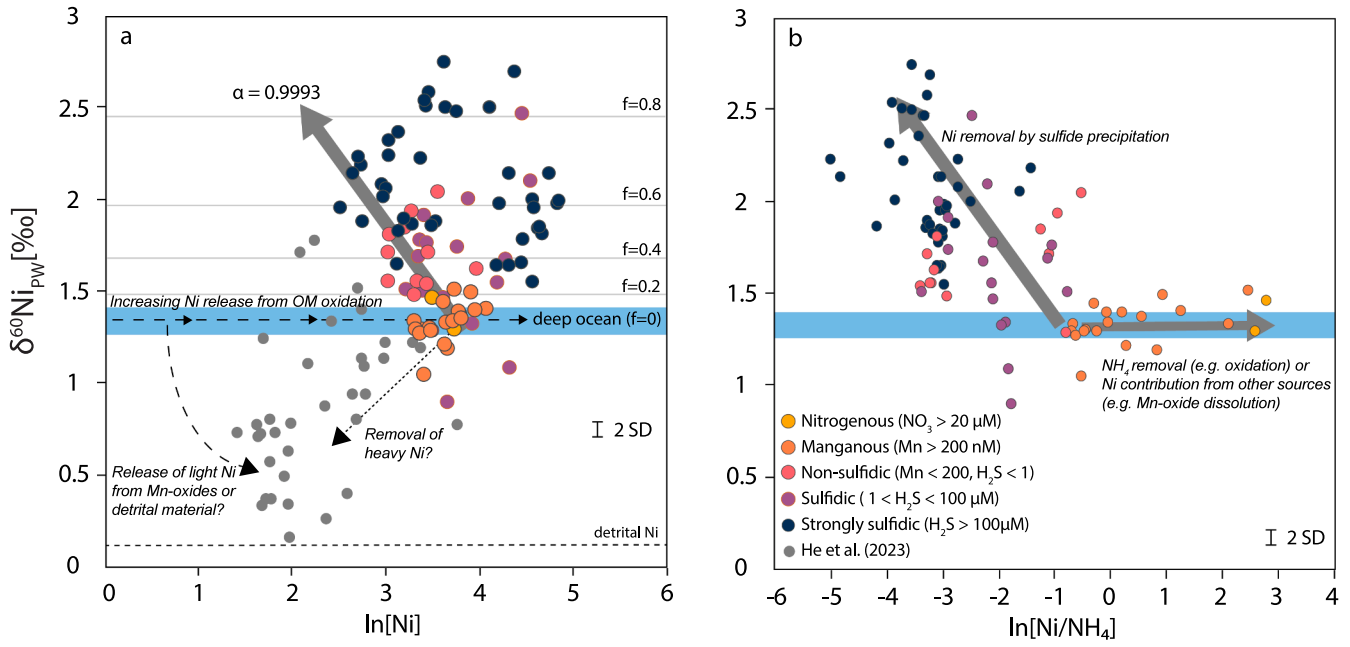

Fig. 8. Pore water δ^{60}Ni and [Ni] in different redox zones. The colours represent different redox zones, based on supporting data. Samples from nitrogenous and Mn-rich conditions allow assessment of processes in absence of the formation of Ni-S complexes. These samples largely cluster around the seawater isotopic composition, suggesting that Ni released from the remineralisation of organic matter is mostly unfractionated from seawater. Samples from progressively more sulphidic conditions generally show progressively higher δ^{60}Ni values. For a group of samples, the trend in δ^{60}Ni vs ln[Ni] from nitrogenous to strongly sulphidic conditions is consistent with an α of 0.9993, calculated using *ab initio* methods and fitting with sulphidic deep Black Sea δ^{60}Ni data (Fujii et al., 2014; Vance et al., 2016), suggesting precipitation of isotopically light Ni-S complexes from sulphidic pore waters with an initial deep-ocean composition. However, this model does not describe the overall trend and there is considerable scatter in the data. This scatter can at least partly be partly be attributed to the variable release of Ni from organic matter oxidation, with a δ^{60}Ni value around the deep-ocean composition. Due to the variable Ni release, these data therefore cannot be used to provide better constraints on α. The horizontal grey lines represent the fraction (f) of Ni precipitated as sulphides assuming a Rayleigh fractionation model with an α of 0.9993 and an initial $\delta^{60}Ni_{PW}$ at $f = 0$ of 1.33 ‰. The He et al. (2023) data stand out with relatively low δ^{60}Ni values. These values are likely explained by the contribution of isotopically light Ni from other sedimentary phases (e.g. oxides or lithogenic material) to a smaller dissolved Ni pool. In an effort to correct for variable Ni release from organic matter oxidation, figure (b) shows the Ni concentrations normalised to pore water [NH_4^+] (Fleischmann et al., 2025). While a lot of scatter remains, following this normalization the data from sulphidic conditions generally fit with sulphide precipitation as the key control on pore water δ^{60}Ni and [Ni]. Variation in Ni/NH_4^+ for the non-sulphidic pore waters may be explained by removal of NH_4^+ from pore waters or addition of Ni from sediment sources other than the organic pool, e.g. reductive Mn-oxide dissolution.

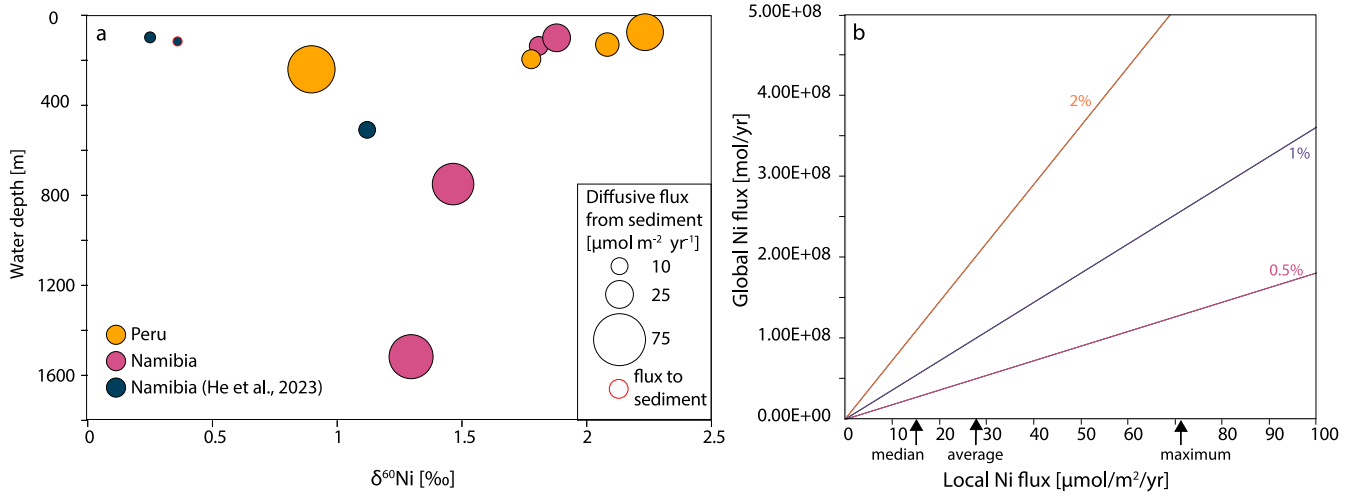

Fig. 9. The benthic flux from continental margin upwelling settings. (a) The size of benthic Ni fluxes and δ^{60}Ni values of the top pore water samples for the Namibian and Peruvian margins. The anoxic shelf stations with high sedimentary Ni contents studied here feature an efflux flux of isotopically heavy Ni from the sediment, whereas δ^{60}Ni values for the benthic flux from the deeper stations approach seawater composition. (b) Estimates of the global size of the recycled benthic flux. Local Ni fluxes out of the sediment as observed for the studied stations are shown on the x-axis. The lines represent the flux from these environments for different surface areas as a percentage of the total seafloor.

the surface sediment on the California margin. However, as noted earlier, this latter study based this conclusion on the assertion that pore water Ni isotope compositions close to 0 ‰ identify a lithogenic Ni contribution, and cannot derive from reductively-dissolved Mn oxide. In fact, the range of Mn-oxide-associated Ni isotope compositions extends from −1 to over +2 ‰. In particular, the range for the Mn-reducing settings studied by Bian et al. (2024b) is −0.79 to +0.09 (Fleischmann et al., 2023; Little et al., 2020), encompassing the lithogenic value.

Importantly, therefore, the benthic flux observed for the stations studied here represents a recycled flux, not a net input to the global dissolved pool. Thus, there is no impact on estimates of outputs from the global ocean that have previously been defined based on the characteristics of buried Ni in sediment (e.g. Ciscato et al., 2018; Fleischmann et al., 2023; Fleischmann et al. 2025). For the Peru margin stations studied here, sediment mass accumulation rates are available from Dale et al. (2021), allowing us to use excess Ni contents to calculate a Ni burial flux (Table S1). These data suggest that 2–24 % of the Ni delivered to these stations is lost from the sediment as benthic efflux, while 76–98 % is buried. Ni burial is least efficient in non-sulphidic sediment redox conditions, with a 76 % burial efficiency found for station 6 on the Peru margin. Overall, these values, with those in Bruggmann et al. (2024) and Fleischmann et al. (2025), suggest highly efficient Ni burial in this setting, at 92±7 % (1SD, $n = 11$).

Nevertheless, the data do suggest that benthic fluxes from sediment to seawater are a significant feature of highly-productive continental margin environments. The processes we identify in this study occur in settings with high OM deposition rates and sulphidic pore waters at depth. Literature estimates for the area of such settings vary from about 0.3–1.9 % of the global ocean (e.g., Carr, 2001; Chen et al., 2015; Reinhard et al., 2013; Scott et al., 2008). Fig. 9b shows the global benthic flux implied by a similar range of areas, given the median and average fluxes for the studied stations. Fleischmann et al. (2025) estimate a total (global) burial flux of Ni in these settings of 1.54×10^8 mol/yr. This, as well as the burial efficiency of 92±7 % estimated above, provides a different estimate of the size of the global benthic efflux, of no more than about 0.3×10^8 mol/ yr. This would be consistent with the median/average benthic flux obtained here, given the lower end of the range of areas cited above (0.3/0.5 %, Fig. 9b).

Finally, organic carbon rain rates to the sediment-water interface are also available for the Peru margin stations, (Dale et al., 2015). These, along with the Ni/C ratio for uptake implied by Ni/P ratios for diatoms (equivalent to Ni/C ~ 5–15 μmol/mol; Twining and Baines, 2013), and by the water column measurements used to constrain global Ni/P uptake ratios in Fig. 5 (equivalent to Ni/C ~ 9–17 μmol/mol; Twining and Baines, 2013), can be used to calculate Ni delivery rates. These estimates present us with somewhat of a mass balance problem. For Peru stations 1 and 3, estimates of Ni delivery to the sediment-water interface derived in this way amount to 50–100 % of the sum of the burial and benthic fluxes which, given the uncertainties involved, seems like reasonable agreement. However, for stations 5 and 6, only 10–15 % of the sum of the burial and benthic fluxes can be explained by the organic carbon rain rate and these Ni/C ratios. Whether this is due to issues with estimates of organic matter rain rate, other sources of Ni to the sediment, or increases in Ni/C ratios of organic matter on passage downward through the water column is difficult to assess. More efforts combining detailed reconstructions of accumulation rates, benthic fluxes, and water column particulate data would shed more light on this issue.

6. Conclusion

We present a large dataset of sediment and pore water δ^{60}Ni data from a range of depositional redox conditions in highly productive upwelling margins. These data show that excess Ni associated with organic-carbon burial in these settings is unfractionated from the deep ocean, with an average $\delta^{60}Ni_{excess}$ of 1.37 ± 0.16 ‰ (1 SD, $n = 74$) for Ni-enriched ($f_{excess} > 0.8$) samples, assuming a maximum Ni/Al_{lith} of 5.8×10^{-4} for all available data. Organic-rich margin sediments from the sedimentary record can thus be used as a suitable archive for the δ^{60}Ni of past oceans. Pore water data suggest that Ni release from excess Ni phases generally does not lead to isotope fractionation in these settings, with pore water δ^{60}Ni values in nitrogenous and Mn-rich conditions also varying around the seawater composition. In more reducing pore waters, the preferential removal of isotopically light Ni leaves sulphidic pore waters enriched in isotopically heavy Ni (δ^{60}Ni of 2.04 ± 0.41, 1 SD, $n = 43$ in strongly sulphidic conditions). As previously suggested (He et al., 2023; Bruggmann et al., 2024; Fleischmann et al., 2025), the solid Ni phase dominates the mass-balance of the sediment-pore water system, so that isotope fractionation of the dissolved pool does not significantly affect the sedimentary excess Ni isotope composition. Pore water Ni concentrations are generally higher than seawater concentrations, and positively correlated with sedimentary Ni contents. The high pore water concentrations imply a recycled benthic flux of isotopically heavy Ni out of the sediment from these environments, with average and maximum fluxes of −28 and −71 μmol m^{-2} yr^{-1} of Ni, respectively. These fluxes are locally significant, especially where sediment redox conditions are non-sulphidic, but relatively small compared to the Ni accumulation rates, suggesting that Ni burial in these environments is generally relatively efficient. Additionally, as this benthic flux largely consists of recycled excess Ni it is not a net input to the global Ni mass balance.

Figure S1 Sampling locations in the Namibian margin, map by Kraal et al., (2025)

Figure S2 Sampling locations in the Peruvian margin, map by Plass et al., (2021)

Figure S3 $\delta^{60}Ni_{excess}$ as a function of f_{excess}. Calculated $\delta^{60}Ni_{excess}$ values converge to the deep ocean composition with higher excess Ni fractions (f_{excess}) for the productive upwelling stations. The Ni/Al of 3.3×10^{-4} used for the lithogenic corrections (left panel) likely overestimates lithogenic Ni contributions to the Peru Margin samples; a lower Ni/Al value 1.7×10^{-4} may be used for those samples (right panel) (Böning et al., 2012). [1]This study; [2]Ciscato et al. (2018); [3]He et al. (2023); [4]Vance et al. (2016).

Figure S4 Ni-TOC relationship of productive margin sediments. The data presented here fits the previously observed Ni-TOC correlation with a gradient of $\sim 9 \times 10^{-4}$ [g/g] (Böning et al., 2015; Ciscato et al., 2018).

Table S1: Summary of benthic and Ni burial (only available for Peru) fluxes from Peru and Namibian margin stations

CRediT authorship contribution statement

Tim Sweere: Writing – review & editing, Writing – original draft, Visualization, Resources, Methodology, Investigation, Funding acquisition, Conceptualization. **Corey Archer:** Writing – review & editing, Visualization, Methodology, Investigation. **Sarah Fleischmann:** Investigation. **Florian Scholz:** Writing – review & editing, Resources. **Peter Kraal:** Writing – review & editing, Resources. **Derek Vance:** Writing – review & editing, Supervision, Conceptualization.

Declaration of competing interest

The authors declare that they have no known competing financial interests or personal relationships that could have appeared to influence the work reported in this article

Acknowledgements

We kindly thank the crews and scientists aboard the RV Pelagia and RV Meteor during cruises 64PE449, M136, and M137 for facilitating the collection of all sampled material. Specifically, we thank Karel Bakker, Kristin Ungerhofer, Fabienne Berger, Lars Krause, Nolwenn Lemaitre, and Anna Plass for their contributions during an early stage of the project. Sampling on the Peruvian margin was financially supported by

the German Research Foundation through the Emmy Noether Research Group ICONOX (Iron Cycling in Continental margin Sediments and the Nutrient and Oxygen Balance of the Ocean) and Collaborative Research Center 754 (Climate-Biogeochemistry Interactions in the Tropical Ocean). TCS has received funding from the European Union's Horizon 2020 research and innovation program under the Marie Skłodowska-Curie grant agreement No. 834236. We thank the editor and two anonymous reviewers for their helpful and constructive comments that have considerably improved our manuscript.

Supplementary materials

Supplementary material associated with this article can be found, in the online version, at doi:10.1016/j.epsl.2025.119549.

Data availability

The data can be found in the supplementary files.

References

Alfano, M., Cavazza, C., 2020. Structure, function, and biosynthesis of nickel-dependent enzymes. Protein Sci. 29 (5), 1071–1089.
Archer, C., Vance, D., Milne, A., Lohan, M.C., 2020. The oceanic biogeochemistry of nickel and its isotopes: new data from the South Atlantic and the Southern Ocean biogeochemical divide. Earth. Planet. Sci. Lett. 535, 116118.
Bian, X., Yang, S.C., Raad, R.J., Odendahl, C.E., Lanning, N.T., Sieber, M., Huang, K.F., Fitzsimmons, J.N., Conway, T.M., John, S.G., 2024a. Distribution and cycling of nickel and nickel isotopes in the Pacific Ocean. Geophys. Res. Lett. 51, e2024GL111115.
J. F. Bian, X., Yang, S.C., Raad, R.J., Lunstrum, A.M., Dong, S., Meng, H., Kemnitz, N., Rollins, N.E., Cetiner, J.E.P., Pavia, F.J., Hammond, D., Adkins, E., Berelson, W.M., John, S.G, 2024b. A benthic source of isotopically heavy Ni from continental margins and implications for global ocean Ni isotope mass balance Earth Planet. Sci. Lett. 645, 118951.
Böning, P., Fröllje, H., Beck, M., Schnetger, B., Brumsack, H.J., 2012. Underestimation of the authigenic fraction of Cu and Ni in organic-rich sediments. Mar. Geol 323, 24–28.
Böning, P., Shaw, T., Pahnke, K., Brumsack, H.J., 2015. Nickel as indicator of fresh organic matter in upwelling sediments. Geochim. Cosmochim. Acta 162, 99–108.
Boudreau, B.P., 1996. The diffusive tortuosity of fine-grained unlithified sediments. Geochim. Cosmochim. Acta 60 (16), 3139–3142.
Boudreau, B.P., 1997. Diagenetic Models and Their Implementation, 505. Springer, Berlin.
Bruggmann, S., McManus, J., Archer, C., Vance, D., Severmann, S., 2024. Nickel's behaviour in marine sediments under aerobic to anaerobic diagenetic conditions. Chemical Geology 662, 122234. https://doi.org/10.1016/j.chemgeo.2024.122234.
Bruland, K.W., 1980. Oceanographic distributions of cadmium, zinc, nickel, and copper in the North Pacific. Earth Planet. Sci. Lett. 47 (2), 176–198.
Calvert, S.E., Price, N.B., 1983. Geochemistry of Namibian shelf sediments. In: Suess, E., Thiede, J. (Eds.), Coastal Upwelling Its Sediment Record: Part A: Responses of the Sedimentary Regime to Present Coastal Upwelling. Springer US, Boston, MA, pp. 337–375.
Cameron, V., Vance, D., 2014. Heavy nickel isotope compositions in rivers and the oceans. Geochim. Cosmochim. Acta 128, 195–211.
Cameron, V., Vance, D., Archer, C., House, C.H., 2009. A biomarker based on the stable isotopes of nickel. Proc. Natl. Acad. Sci. 106 (27), 10944–10948.
Carr, M.E., 2001. Estimation of potential productivity in Eastern Boundary Currents using remote sensing. Deep Sea Res. II 49 (1–3), 59–80.
Chen, X., Ling, H.F., Vance, D., Shields-Zhou, G.A., Zhu, M., Poulton, S.W., Och, L.M., Jiang, S.Y., Li, D., Cremonese, L., Archer, C., 2015. Rise to modern levels of ocean oxygenation coincided with the cambrian radiation of animals. Nat. Commun. 6 (1), 7142.
Ciscato, E.R., Bontognali, T.R., Vance, D., 2018. Nickel and its isotopes in organic-rich sediments: implications for oceanic budgets and a potential record of ancient seawater. Earth Planet. Sci. Lett. 494, 239–250.
Cline, J.D., 1969. Spectrophotometric determination of hydrogen sulphide in natural waters. Limnol. Ocean. 14, 454–458.
Dale, A.W., Sommer, S., Lomnitz, U., Montes, I., Treude, T., Liebetrau, V., Gier, J., Hensen, C., Dengler, M., Stolpovsky, K., Bryant, L.D., 2015. Organic carbon production, mineralisation and preservation on the Peruvian margin. Biogeosciences 12 (5), 1537–1559.
Dale, A.W., Paul, K.M., Clemens, D., Scholz, F., Schroller-Lomnitz, U., Wallmann, K., Geilert, S., Hensen, C., Plass, A., Liebetrau, V., Grasse, P., 2021. Recycling and burial of biogenic silica in an open margin oxygen minimum zone. Glob. Biogeochem. Cycles 35 (2), e2020GB006583.
Dengler, M., Sommer, S., 2017. Coupled Benthic and Pelagic oxygen, Nutrient and Trace Metal cycling, Ventilation and Carbon Degradation in the Oxygen Minimum Zone of the Peruvian continental Margin (SFB 754): Cruise No. M 136 11.04.–03.05. 2017 Callao (Peru)–Callao Solute-Flux Peru I.
Dupont, C., Neupane, K., Shearer, J., Palenik, B., 2008. Diversity, function and evolution of genes coding for putative Ni-containing superoxide dismutases. Env.. Microbiol 10 (7), 1831–1843.
Dupont, C.L., Buck, K.N., Palenik, B., Barbeau, K., 2010. Nickel utilization in phytoplankton assemblages from contrasting oceanic regimes. Deep Sea Res. I 57 (4), 553–566.
Fleischmann, S., Du, J., Chatterjee, A., McManus, J., Iyer, S.D., Amonkar, A., Vance, D., 2023. The nickel output to abyssal pelagic manganese oxides: a balanced elemental and isotope budget for the oceans. Earth Planet. Sci. Lett. 619, 118301.
Fleischmann, S., Scholz, F., Du, J., Scholten, J., Vance, D., 2025. Processes controlling nickel and its isotopes in anoxic sediments of a seasonally hypoxic bay. Geochim. Cosmochim. Acta 391, 1–15.
Fujii, T., Moynier, F., Blichert-Toft, J., Albarède, F., 2014. Density functional theory estimation of isotope fractionation of Fe, Ni, Cu, and Zn among species relevant to geochemical and biological environments. Geochim. Cosmochim. Acta 140, 553–576.
Gall, L., Williams, H., Siebert, C., Halliday, A., Herrington, R., Hein, J., 2013. Nickel isotopic compositions of ferromanganese crusts and the constancy of deep ocean inputs and continental weathering effects over the Cenozoic. Earth Planet. Sci. Lett. 375, 148–155.
Gäng, F., Böning, P., Brüchert, V., Lahajnar, N., Pahnke, K., 2023. Critical assessment of U, Ba and Ni as redox and productivity proxies in organic-rich sediments underneath dynamic, highly productive waters. Geochimica et Cosmochimica Acta 348, 206–220.
Glass, J., Dupont, C., 2017. Oceanic nickel biogeochemistry and the evolution of nickel use. Biol. Chem. Nickel 12–26.
Gueguen, B., Rouxel, O., 2021. The nickel isotope composition of the authigenic sink and the diagenetic flux in modern oceans. Chem. Geol. 563, 120050.
He, Z., Archer, C., Yang, S., Vance, D., 2023. Sedimentary cycling of zinc and nickel and their isotopes on an upwelling margin: implications for oceanic budgets and paleoenvironment proxies. Geochim. Cosmochim. Acta 343, 84–97.
Ho, T.Y., 2013. Nickel limitation of nitrogen fixation in Trichodesmium. Limnol. Ocean. 58 (1), 112–120.
Inthorn, M., Wagner, T., Scheeder, G., Zabel, M., 2006. Lateral transport controls distribution, quality, and burial of organic matter along continental slopes in high-productivity areas. Geology 34 (3), 205–208.
Jacobs, L., Emerson, S., Skei, J., 1985. Partitioning and transport of metals across the O2H2S interface in a permanently anoxic basin: framvaren Fjord, Norway. Geochim. Cosmochim. Acta 49 (6), 1433–1444.
John, S.G., Kelly, R.L., Bian, X., Fu, F., Smith, M.I., Lanning, N.T., Holzer, M., 2022. The biogeochemical balance of oceanic nickel cycling. Nat. Geosci. 15 (11), 906–912.
Konhauser, K.O., Pecoits, E., Lalonde, S.V., Papineau, D., Nisbet, E.G., Barley, M.E., Kamber, B.S., 2009. Oceanic nickel depletion and a methanogen famine before the great oxidation event. Nature 458 (7239), 750–753.
Kraal, P., Ungerhofer, K.A., Rush, D., Reichart, G.J., 2025. Benthic phosphorus cycling in the northern Benguela upwelling system: excess P supply and altered pelagic nutrient stoichiometry. Biogeosciences 1–39.
Landing, W.M., Lewis, B.L., 1991. Thermodynamic modeling of trace metal speciation in the Black Sea. Black Sea Oceanogr. 125–160.
Lemaitre, N., Du, J., De Souza, Archer, C., Vance, D., 2022. The essential bioactive role of nickel in the oceans: Evidence from nickel isotopes. Earth and Planetary Science Letters 584, 117513.
Little, S.H., Archer, C., McManus, J., Najorka, J., Wegorzewski, A.V., Vance, D., 2020. Towards balancing the oceanic Ni budget. Earth Planet. Sci. Lett. 547, 116461.
Mackey, D., O'Sullivan, J., Watson, R., Dal Pont, G., 2002. Trace metals in the Western Pacific: temporal and spatial variability in the concentrations of Cd, Cu, Mn and Ni. Deep Sea Res. I 49 (12), 2241–2259.
Middag, R., De Baar, H.J., Bruland, K.W., Van Heuven, S.M., 2020. The distribution of nickel in the West-Atlantic Ocean, its relationship with phosphate and a comparison to cadmium and zinc. Front. Mar. Sci. 7, 105.
Morel, F., Milligan, A., Saito, M., 2006. Marine Bioinorganic Chemistry: the. Oceans Mar. Geochem. 6, 113.
Morse, J.W., Luther Iii, G.W., 1999. Chemical influences on trace metal-sulphide interactions in anoxic sediments. Geochim. Cosmochim. Acta 63 (19–20), 3373–3378.
Plass, A., Dale, A.W., Scholz, F., 2021a. Sedimentary cycling and benthic fluxes of manganese, cobalt, nickel, copper, zinc and cadmium in the Peruvian oxygen minimum zone. Mar. Chem. 233, 103982.
Plass, A., Schlosser, C., Sommer, S., Dale, A.W., Achterberg, E.P., Scholz, F., 2021b. The control of hydrogen sulphide on benthic iron and cadmium fluxes in the oxygen minimum zone off Peru. Biogeosciences 17 (13), 3685–3704.
Price, N., Morel, F.M., 1991. Colimitation of phytoplankton growth by nickel and nitrogen. Limnol. Ocean. 36 (6), 1071–1077.
Ragsdale, S.W., 2009. Nickel-based enzyme systems. J. Biol. Chem. 284 (28), 18571–18575.
Reinhard, C.T., Planavsky, N.J., Robbins, L.J., Partin, C.A., Gill, B.C., Lalonde, S.V., Bekker, A., Konhauser, K.O., Lyons, T.W., 2013. Proterozoic ocean redox and biogeochemical stasis. Proc. Natl. Acad. Sci. 110 (14), 5357–5362.
Revels, B.N., Rickli, J., Moura, C.A., Vance, D., 2021. Nickel and its isotopes in the Amazon Basin: the impact of the weathering regime and delivery to the oceans. Geochim. Cosmochim. Acta 293, 344–364.
Rudnick, R.L., Gao, S., 2003. Composition of the continental crust. Treatise on Geochemistry 1–64.
Scheller, S., Goenrich, M., Boecher, R., Thauer, R.K., Jaun, B., 2010. The key nickel enzyme of methanogenesis catalyses the anaerobic oxidation of methane. Nature 465 (7298), 606–608.

Sclater, F., Boyle, E., Edmond, J., 1976. On the marine geochemistry of nickel. Earth Planet. Sci. Lett. 31 (1), 119–128.
Scholz, F., Hensen, C., Noffke, A., Rohde, A., Liebetrau, V., Wallmann, K., 2011. Early diagenesis of redox-sensitive trace metals in the Peru upwelling area–response to ENSO-related oxygen fluctuations in the water column. Geochim. Cosmochim. Acta 75 (22), 7257–7276.
Schunck, H., Lavik, G., Desai, D.K., Großkopf, T., Kalvelage, T., Löscher, C.R., Paulmier, A., Contreras, S., Siegel, H., Holtappels, M., Rosenstiel, P., 2013. Giant hydrogen sulphide plume in the oxygen minimum zone off Peru supports chemolithoautotrophy. PLoS. One 8 (8), e68661.
Scott, C., Lyons, T.W., Bekker, A., Shen, Y.A., Poulton, S.W., Chu, X.L., Anbar, A.D., 2008. Tracing the stepwise oxygenation of the proterozoic ocean. Nature 452 (7186), 456–459.
Sommer, S., Dengler, M., 2019. Benthic Element cycling, Fluxes and Transport of Nutrients and Trace Metals Across the Benthic Boundary Layer in the Peruvian oxygen Minimum Zone (SFB 754), Cruise No. 137, 06.05.–29.05. 2017 Callao (Peru)–Callao.
Suess, E., Kulm, L.D., Killingley, J.S., 1987. Coastal upwelling and a history of organic-rich mudstone deposition off Peru. Geol. Soc. 26 (1), 181–197.
Sun, M., Archer, C., Scholz, F., Sweere, T., Vance, D., 2025. Trace metal evolution of the late cretaceous Ocean. Chem. Geol. 671, 122477.
Sun, M., Archer, C., Vance, D., 2021. New methods for the chemical isolation and stable isotope measurement of multiple transition metals, with application to the earth sciences. Geostand. Geoanalytical Res. 45 (4), 643–658.
Sweere, T.C., Dickson, A.J., Vance, D., 2023. Nickel and zinc micronutrient availability in phanerozoic oceans. Geobiology 21 (3), 310–322.
Takano, S., Tanimizu, M., Hirata, T., Shin, K.C., Fukami, Y., Suzuki, K., Sohrin, Y., 2017. A simple and rapid method for isotopic analysis of nickel, copper, and zinc in seawater using chelating extraction and anion exchange. Anal. Chim. Acta 967, 1–11.
Thamdrup, B., Dalsgaard, T., Revsbech, N.P., 2012. Widespread functional anoxia in the oxygen minimum zone of the Eastern South Pacific. Deep Sea Res. I 65, 36–45.
Twining, B.S., Baines, S.B., 2013. The trace metal composition of marine phytoplankton. Ann. Rev. Mar. Sci. 5, 191–215.
van Kemenade, Z.R., Villanueva, L., Hopmans, E.C., Kraal, P., Witte, H.J., Sinninghe Damsté, J.S., Rush, D., 2022. Bacteriohopanetetrol-x: constraining its application as a lipid biomarker for marine anammox using the water column oxygen gradient of the Benguela upwelling system. Biogeosciences 19 (1), 201–221.
Vance, D., Little, S.H., Archer, C., Cameron, V., Andersen, M.B., Rijkenberg, M.J., Lyons, T.W., 2016. The oceanic budgets of nickel and zinc isotopes: the importance of sulphidic environments as illustrated by the Black Sea. Philos. Trans. R. Soc. A 374 (2081), 20150294.
Wang, R.M., Archer, C., Bowie, A.R., Vance, D., 2019a. Zinc and nickel isotopes in seawater from the Indian Sector of the Southern Ocean: the impact of natural iron fertilization versus Southern Ocean hydrography and biogeochemistry. Chem. Geol 511, 452–464.
Wang, S.J., Rudnick, R.L., Gaschnig, R.M., Wang, H., Wasylenki, L.E., 2019b. Methanogenesis sustained by sulphide weathering during the Great Oxidation Event. Nat. Geosci. 12 (4), 296–300.
Weeks, S.J., Currie, B., Bakun, A., Peard, K.R., 2004. Hydrogen sulphide eruptions in the Atlantic Ocean off southern Africa: implications of a new view based on SeaWiFS satellite imagery. Deep Sea Res. I 51 (2), 153–172.
Yang, S.C., Hawco, N.J., Pinedo-González, P., Bian, X., Huang, K.F., Zhang, R., John, S. G., 2020. A new purification method for Ni and Cu stable isotopes in seawater provides evidence for widespread Ni isotope fractionation by phytoplankton in the North Pacific. Chem. Geol 547, 119662.
Yang, S.C., Kelly, R.L., Bian, X., Conway, T.M., Huang, K.F., Ho, T.Y., Neibauer, J.T., Keil, R.G., Moffett, J.W., John, S.G., 2021. Lack of redox cycling for nickel in the water column of the eastern tropical north pacific oxygen deficient zone: insight from dissolved and particulate nickel isotopes. Geochim. Cosmochim. Acta 309, 235–250.
Yuan-Hui, L., Gregory, S., 1974. Diffusion of ions in sea water and in deep-sea sediments. Geochim. Cosmochim. Acta 38 (5), 703–714.